Presentation of microstructural diffusion components by color schemes in abdominal organs

Hans-Jörg Wittsack, Thomas Andreas Thiel, Birte Valentin, Julia Stabinska, Thomas Benkert, Lars Schimmöller, Gerald Antoch, Alexandra Ljimani

Article - Version of Record

Received: 20 March 2024 | Revised: 24 April 2024 | Accepted: 17 May 2024

DOI: 10.1002/mrm.30183

Magnetic Resonance in Medicine

TECHNICAL NOTE

Presentation of microstructural diffusion components by color schemes in abdominal organs

Hans-Jörg Wittsack[1] | **Thomas Andreas Thiel**[1] | **Birte Valentin**[1] | **Julia Stabinska**[2] | **Thomas Benkert**[3] | **Lars Schimmöller**[1,4] | **Gerald Antoch**[1] | **Alexandra Ljimani**[1,5]

[1]Department of Diagnostic and Interventional Radiology, Medical Faculty and University Hospital Düsseldorf, Heinrich-Heine-University Düsseldorf, Düsseldorf, Germany

[2]F.M. Kirby Research Center for Functional Brain Imaging, Kennedy Krieger Institute, Baltimore, Maryland, USA

[3]MR Applications Predevelopment, Siemens Healthineers AG, Forchheim, Germany

[4]Department of Diagnostic, Interventional Radiology and Nuclear Medicine, Marien Hospital Herne, University Hospital of the Ruhr-University Bochum, Herne, Germany

[5]Center for Integrated Oncology (CIO Aachen, Bonn, Cologne, Duesseldorf), Aachen, Bonn, Cologne, Düsseldorf, Germany

Correspondence
Hans-Jörg Wittsack, Department of Diagnostic and Interventional Radiology, Medical Faculty, University Dusseldorf, Moorenstr. 5, 40225 Düsseldorf, Germany.
Email: hans-joerg.wittsack@med.uni-duesseldorf.de

Funding information
Deutsche Forschungsgemeinschaft, Grant/Award Numbers: 408765040, 497764939

Abstract

Purpose: Development of a color scheme representation to facilitate the interpretation of tri-exponential DWI data from abdominal organs, where multi-exponential behavior is more pronounced.

Methods: Multi-exponential analysis of DWI data provides information about the microstructure of the tissue under study. The tri-exponential signal analysis generates numerous parameter images that are difficult to analyze individually. Summarized color images can simplify at-a-glance analysis. A color scheme was developed in which the slow, intermediate, and fast diffusion components were each assigned to a different red, green, and blue color channel. To improve the appearance of the image, histogram equalization, gamma correction, and white balance were used, and the processing parameters were adjusted. Examples of the resulting color maps of the diffusion fractions of healthy and pathological kidney and prostate are shown.

Results: The color maps obtained by the presented method show the merged information of the slow, intermediate, and fast diffusion components in a single view. A differentiation of the different fractions becomes clearly visible. Fast diffusion regimes, such as in the renal hilus, can be clearly distinguished from slow fractions, such as in dense tumor tissue.

Conclusion: Combining the diffusion information from tri-exponential DWI analysis into a single color image allows for simplified interpretation of the diffusion fractions. In the future, such color images may provide additional information about the microstructural nature of the tissue under study.

KEYWORDS

abdominal organs, color image, diffusion fraction, DWI, RGB color image, tri-exponential

1 | INTRODUCTION

Diffusion-weighted MRI (DWI) has become a versatile diagnostic tool for detecting and characterizing various types of pathology, such as cancer, fibrosis, or ischemia.[1–4] DWI provides unique structural and functional information that complements the excellent anatomical detail offered by conventional MRI. DWI image contrast depends on the microscopic molecular mobility of water molecules, which is directly influenced by the cellular structure of the tissue. In addition to the restrictions of free diffusion through cell membranes and macromolecules, microscopic directed flow also affects the DWI signal.[5] Recent studies have focused on analyzing the various factors that influence DWI to obtain more information about the microstructure and function of the tissue under study.[6] In the kidney, a tri-exponential diffusion model has recently been proposed to account for three fractions of diffusion regimes: slow tissue diffusion, intermediate pseudo-diffusion in renal tubules, and fast pseudo-diffusion of the blood compartment.[7–9] In brain tissue, three exponential components were attributed to the perfusion-related diffusion, fast-free diffusion, and slow-restricted diffusion.[10] The tri-exponential behavior of the DWI signal also appears to be present in other organs and to contain diagnostic information.[1,11,12]

To disentangle the three diffusion components present in the diffusion MR signal, DWI data are acquired at multiple diffusion weightings (b-values). The pixel-wise tri-exponential fit of the diffusion-weighted signal across the b-values produces six different parameter maps, namely, the signal fraction maps and the corresponding (pseudo-) diffusion coefficient maps for each of the three components. Consequently, the visual analysis of the fitting results is more difficult compared with other single-contrast MRI modalities.

In the present study, we introduce an alternative color-coded visualization method that integrates the information on diffusion fractions into a single parametric image, thus facilitating the interpretation of the multiparametric DWI results. Some representative color maps are shown to illustrate the ease of reading and benefits of the proposed approach when analyzing the results of tri-exponential DWI analysis.

2 | METHODS

2.1 | Tri-exponential model

A commonly used tri-exponential model for DWI is as follows:

$$S(b)/S_0 = \left(f_s \cdot e^{-bD_s} + f_i \cdot e^{-bD_i} + f_f \cdot e^{-bD_f}\right) \quad (1)$$

where $S(b)$ and S_0 are signal intensities at a given b-value and without diffusion weighting, respectively.[13] The values of f_s, f_i, and f_f are the fractions of the slow, intermediate, and fast diffusion components (where $f_s = 1 - f_i - f_f$) characterized by the corresponding diffusion constants D_s, D_i, and D_f, respectively. To analyze the MR signal pixel by pixel, Eq. (1) is usually fitted to the measured DWI data by a nonlinear least-squares algorithm, resulting in parametric maps containing the fitted values of the parameters D_s, D_i, D_f and f_s, f_i, f_f. The stability of the modeled parameters is highly dependent on the SNR, especially due to the high number of degrees of freedom. Because acquisition time is limited in in vivo studies, DWI data are typically acquired at 16 different b-values or less over a range of approximately 10 min, resulting in a limited SNR. Therefore, special measures like nonlinear least-squares fitting, noise filtering, or a pyramid approach must be taken to stabilize the fitting process and proper starting values must be selected as prior knowledge.[8,12]

2.2 | Color schemes

Several previous studies have shown a large variation of the resulting diffusion constants D_s, D_i, and D_f using the tri-exponential model.[7,14] On the other hand, the fractions f_s, f_i, and f_f showed more stable results and contain relevant information about the underlying tissue structure in addition to the pure diffusion constant.[6,12] Therefore, in the present work we decided to focus only on the color fraction maps.

The range of values of the diffusion fractions f_s, f_i, and f_f analyzed by Eq. (1) is [0.0–1.0] with the side condition that $1 = f_s + f_i + f_f$. The standard representation of a color image is a 24-bit scheme, with an 8-bit range for each red, green, and blue (RGB) color channel. The 8-bit hold integer values range from 0 to 255; therefore, the first step was to convert the individual fractions to values ranging from 0 to 255 by multiplying f_s, f_i, and f_f with 255. To ensure quality, all pixels with a goodness-of-fit $R^2 < 0.5$ were set to zero. Because the generation of RGB images is not about quantitative analysis of real numerical values, but rather about simplified visual representation, several steps were taken to improve the visualization. It should be noted that setting parameters of the processing steps was determined empirically, with the corresponding parameters being varied step by step in each step for optimization. Because the perception of non-quantitative color images is an individual personal dimension, the presented empirically determined adjustments and processing steps should

not be understood as universal but should illustrate a practicable way of processing. The following processing steps were used to improve the diffusion fraction images.

Histogram equalization was performed separately for each color channel to evenly distribute the color values between 0 and 255.[15] Histogram equalization is particularly important for the individual components f_s, f_i, and f_f, as their individual value ranges are very different. To obtain consistent and stable results from the histogram equalization, the target organ of interest should be extracted from the entire image. Because poorly controlled fitting results can occur in regions outside the target organ, histogram equalization is ineffective and results in fluctuating color maps. To improve the color representation, gamma correction was performed again separately for each color channel.[14] The best gamma values for the red, green, and blue channels were found by systematic variation and visual inspection to be $\gamma_r = 2.4$, $\gamma_g = 2.0$, and $\gamma_b = 2.2$.

Due to the noisy nature of DWI data, artifact pixels often appear in the diffusion fraction maps. Therefore, as a final step, white balance correction was performed using the white patch algorithm.[16] A percentile value of 0.6 suppresses the effect of the artifact pixels and achieves a good white balance.[17,18]

All processing steps were developed in Visual C++ 2017 (Microsoft Corporation) in an in-house software. Algorithms for histogram equalization, gamma correction, and white balance have been developed without the use of external libraries. The RGB maps were created in DICOM format using "dcmtk" (https://dcmtk.org/en/), allowing the data to be sent to a picture archiving system for easy and fast data handling and image analysis by radiologists. To make the creation of color-coded diffusion component maps publicly available, an open-source tool will be released soon on Github (https://github.com/MPR-UKD/RGB-tri).

2.3 | Study population

The study was approved by the local ethics committee, and all participants signed written informed consent before the MRI examination. MRI scans of the kidneys and prostate were analyzed as examples. Four of the subjects were diagnosed with papillary renal cell carcinoma (age = X, Y, and Z years). One healthy control (age = 27 years) underwent MRI of the kidneys. In the case of the prostate, 1 healthy control (age = 29 years) and 4 patients with prostate cancer (ages = 80, 80, and 82 years) were studied. Subjects were randomly selected from other studies using DWI as a method for detailed tissue characterization. They were not specifically examined for the present study, as we used the data here only to present the method of color diffusion fraction imaging.

2.4 | Data acquisition and analysis

The MRI scans were performed on a 3T whole-body MRI system (MAGNETOM Prisma; Siemens Healthineers, Forchheim, Germany). In the case of the kidney, a zoomed single-shot EPI research application sequence with reduced volume excitation was used with an 18-channel torso array coil and a 32-channel spine coil with the following acquisition parameters: TR/TE = 4100/70 ms, FOV = 185 × 270 mm^2, matrix size = 112 × 80, voxel size = 2.3 × 2.3 × 4.2 mm^3, number of slices = 14, and b-values = 0, 10, 20, 30, 40, 50, 70, 90, 120, 170, 250, 350, 450, 550, 650, and 750 s/mm^2. For the prostate, a single-shot EPI-DWI research sequence with reduced volume excitation was used to provide small FOV imaging using a 60-channel body coil with the following parameters: TR/TE = 3700/67 ms, FOV = 91 × 150 mm^2, matrix size = 100 × 164, voxel size = 0.915 × 0.915 × 3 mm^3, number of slices = 28, and b-values = 0, 50, 100, 150, 200, 300, 400, 500, 600, 700, 800, 1000, 1200, 1400, 1600, and 1800 s/mm^2. The different DWI protocols for kidney and prostate were chosen because of the different diffusion tissue characteristics and the desired higher spatial resolution in the case of the prostate.

For postprocessing, first image registration was performed using a diffeomorphism-based deformation model ("ANTs," https://stnava.github.io/ANTs/), followed by edge-preserving nonlocal means filtering ("OpenCV," https://opencv.org/) to improve the signal-to-noise of the images.[19] After manual extraction of the kidney or prostate, the actual nonlinear least squares fitting ("levmar," https://users.ics.forth.gr/~lourakis/levmar/) of the tri-exponential model was performed pixel by pixel. In addition to the resulting quantitative parametric images, RGB maps of the diffusion fractions were calculated. All of the processing steps have been implemented in an in-house-developed software using the libraries mentioned previously.

3 | RESULTS

First, the results of the different processing steps are presented. Then, single cases are shown to demonstrate the information content of the new RGB diffusion fraction maps.

Figure 1 illustrates the processing steps to create the merged color maps of the diffusion fractions for tri-exponential DWI analysis of a healthy kidney and a

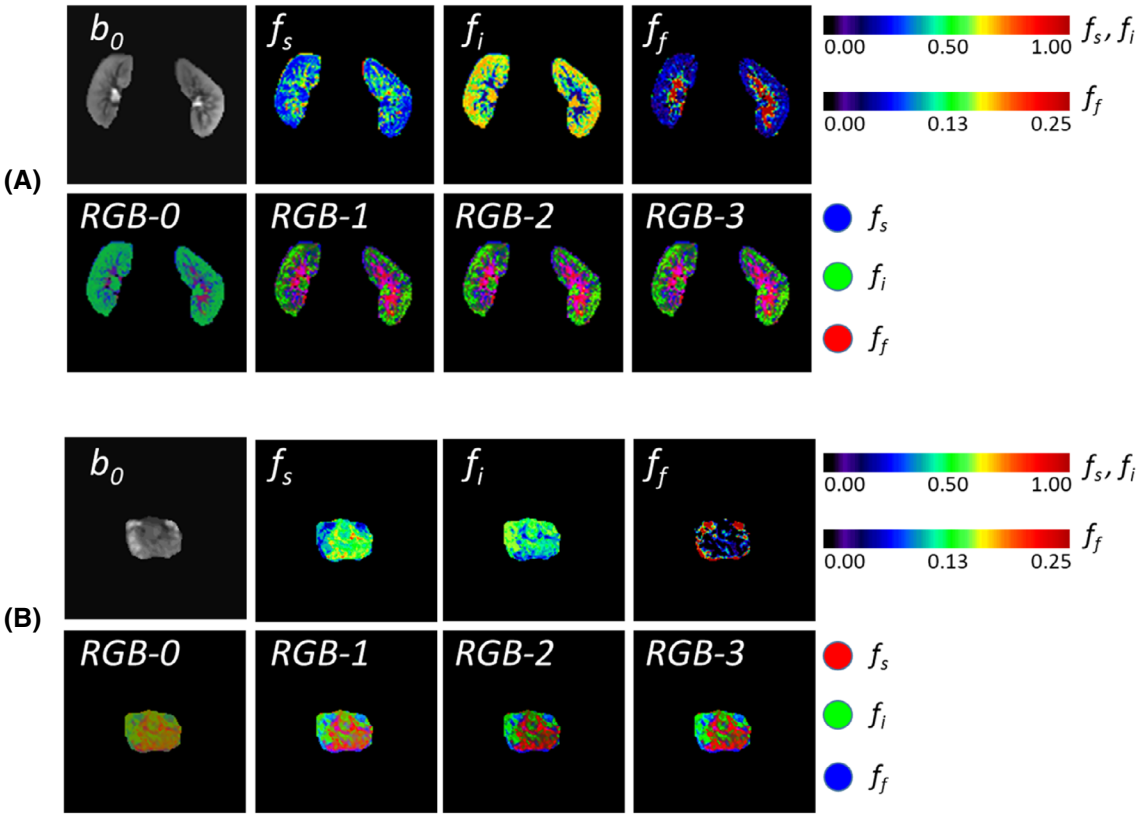

FIGURE 1 Signal fraction maps obtained from the tri-exponential DWI fit in a healthy kidney (A) and prostate (B). The top rows of (A) and (B) show the T_2-weighted image with b-value = 0 mm^2/s and the fractions of the three diffusion components f_s (slow), f_i (intermediate), and f_f (fast). The bottom row in (A) shows the merged red, green, and blue (RGB) maps with f_s (*blue*), f_i (*green*), and f_f (*red*), whereas in (B) the color coding is reversed to f_s (*red*), f_i (*green*), and f_f (*blue*). RGB-0 are the resulting maps without any optimization, RGB-1 after histogram equalization, RGB-2 after histogram equalization, and gamma correction, and RGB-3 after histogram equalization, gamma correction, and white balance.

prostate. Converting diffusion fractions to RGB values alone produces flat, low-contrast color images (RGB-0). The subsequent processing steps of histogram equalization (RGB-1), gamma correction (RGB-2), and white balance (RGB-3) gradually produce the color images of the diffusion fractions. The final color images (RGB-3) show the largest components as the strongest color value compared with the individual quantitative fraction images f_s, f_i, and f_f. In the kidney (Figure 1A; RGB-3), the hilar region with its high flow rate appears in red, corresponding to the largest values of f_f. The renal cortex is shown in green, corresponding to the largest fractions of the intermediate diffusion fraction f_i, possibly due to high tissue perfusion. The central areas shown in blue correspond to the large slow diffusion fractions f_s. In the prostate (Figure 1B; RGB-3) with the reversed color scheme, parts of the peripheral zone are shown in red, corresponding to the highest values of the slow diffusion fraction f_s. Most of the prostate shown in green is due to the large intermediate diffusion component f_i. Because the fast diffusion fraction f_f is low throughout the organ, the blue regions are rather isolated.

Figure 2 shows the effect of organ extraction. The color diffusion fraction maps appear inhomogeneous because of the areas outside the organs where the tri-exponential model fit is not of good quality, possibly due to poor initial parameter guesses. Figure 2A shows a case of renal cancer. Here, the coloring is very flat when the organ is not extracted because there are large differences in the size of fs, fi, and ff in different tissue types and organs throughout the entire abdomen. In Figure 2B, the color map without extraction appears inhomogeneous and difficult to read.

Figure 3 shows examples of colored diffusion fraction images of renal cancer in the top row and prostate cancer in the bottom row.

The kidney tumors showed solid and cystic areas. Within the dense tumor tissue, diffusion is restricted, resulting in a large slow diffusion fraction shown in blue (*yellow arrows in the top row of Figure 3*). The fluid-filled cyst, with its more free diffusion, is shown in green (*red arrows in the top row of Figure 3*), as the intermediate diffusion fraction dominates.

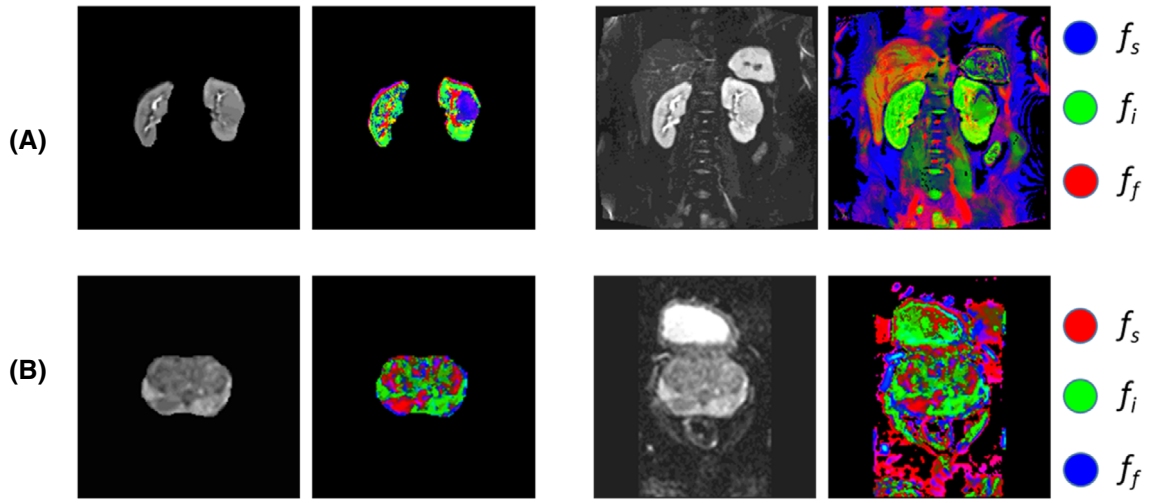

FIGURE 2 Comparison of color diffusion fraction maps from tri-exponential DWI of a cancerous kidney (A) and a cancerous prostate (B) processed with and without organ extraction. The gray scale images show the T_2-weighted images without diffusion weighting; the color images show the diffusion fraction maps as in Figure 1. *Left*: Results with organ extraction. *Right*: Corresponding maps without organ extraction.

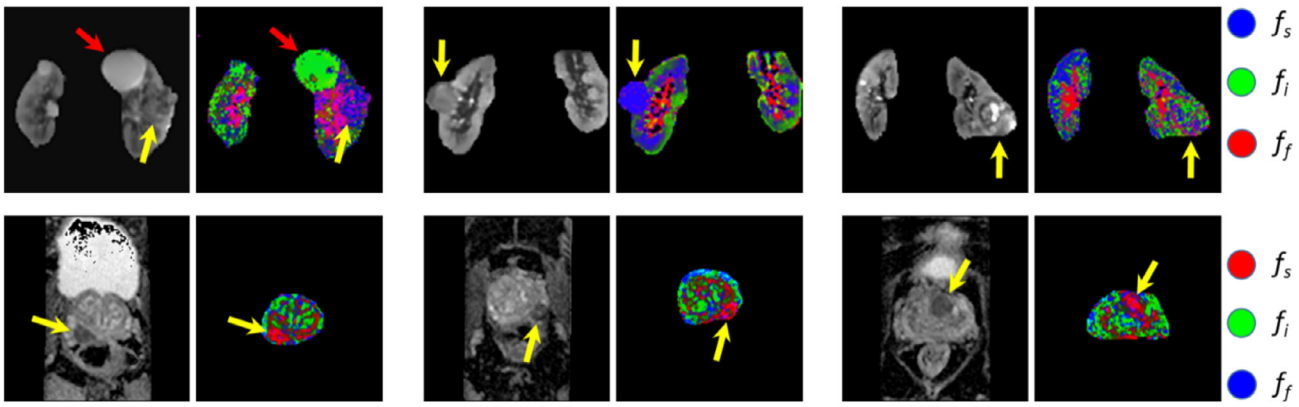

FIGURE 3 Examples of color diffusion fraction images. In the top row, B_0 images alternate with diffusion fraction images of renal tumors. In the bottom row, ADC maps alternate with diffusion fraction images in the prostate. Yellow arrows indicate tumors, and red arrows indicate the location of a cyst.

In the prostate cases, tumors with low ADC values were clearly represented by high fractions of slow diffusion components, shown here in red to highlight the tumor (*yellow arrows in the bottom row of Figure 3*). It should be noted that the information content between ADC and the new diffusion fraction maps is different, as the latter gives information about the fraction of the slow diffusion compartment and not about the decrease of the diffusion constant itself.

Figure 4 shows an enlarged image of a right kidney with a renal tumor for better illustration. The dominant slow diffusion component f_s in the dense tumor tissue is shown in blue, whereas the hilar region is shown in red due to its large flow component f_s.

4 | DISCUSSION

DWI with tri-exponential analysis provides quantitative information about slow, intermediate, and fast diffusion regimes. With its quantitative values of the three diffusion fractions and diffusion constants, the overall information is difficult to interpret. The introduction of color-coded images of diffusion fractions derived from the tri-exponential analysis of DWI data facilitates visual analysis and interpretation of the complex information. As in spectral diffusion analysis, the fractions of the different diffusion compartments provide new information in addition to the pure values of the diffusion constants.[1,8,12] The information content is closer to microstructural tissue compartments and functional measures such as directional flow.

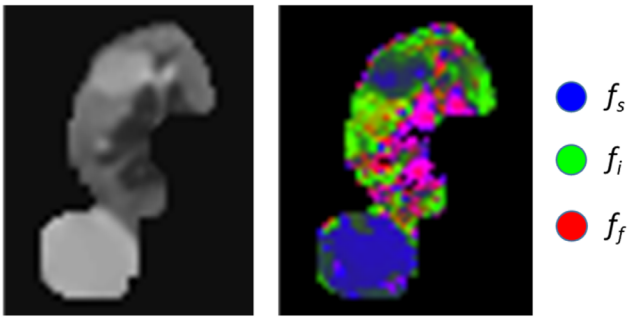

FIGURE 4 Diffusion fraction image of a right kidney with renal tumors. The left image shows the T_2-weighted image with b-value = 0 mm^2/s. In the diffusion fraction image on the right, the renal tumors are reproduced in blue due to the largest component of slow diffusion f_s in the dense tissue. The hilar region is marked in red due to its high flow rates and therefore the largest component f_f.

Therefore, the delineation of diffusion fraction images could help to obtain additional information about the tissue characteristics, possibly with the future goal of tumor classification. Of course, the difficulties associated with a low SNR in DWI need to be considered. Only DWI acquisitions with a good SNR and a sufficient number of b-values, as well as the use of advanced signal modeling techniques, will lead to robust and reliable parameter estimates under the tri-exponential model.[13,14,19,20]

The approach presented here should not be viewed as the only and final method. In fact, it should demonstrate a well-functioning procedure to generate color maps that greatly facilitate the interpretation of tri-exponential diffusion information on a single view. van Baalen et al. also showed merged RGB fraction images, but no further details of their creation were described.[9]

Merging multiple types of information into a single color image has been successful in other modalities. In DTI, color images of fractional anisotropy additionally contain information of axonal fiber directions with their red, green, and blue color channels.[21] These maps have already been proven useful in routine diagnostics. Furthermore, color images have been applied to identify different tissue fractions derived from multishell DWI.[22,23] Perhaps the color images of diffusion fractions proposed here could be useful for more advanced tissue characterization. To analyze the diagnostic value of color diffusion fraction maps, further studies with larger numbers of patients and different pathologies in different organs should be performed.

5 | CONCLUSION

The diffusion information from the tri-exponential DWI analysis merged into a single color image facilitates the interpretation of diffusion fractions. In the future, such colored images may provide additional information on the tissue microstructure in various pathologies.

ACKNOWLEDGMENT

This study was supported by grants from the Deutsche Forschungsgemeinschaft (DFG, German Research Foundation) (Grant/Award Nos. 408765040 and 497764939). Open Access funding enabled and organized by Projekt DEAL.

ORCID

Hans-Jörg Wittsack https://orcid.org/0000-0002-5830-423X
Julia Stabinska https://orcid.org/0000-0003-2730-4250
Alexandra Ljimani https://orcid.org/0000-0002-9748-9927

REFERENCES

1. Ueda Y, Takahashi S, Ohno N, et al. Triexponential function analysis of diffusion-weighted MRI for diagnosing prostate cancer. *J Magn Reson Imaging.* 2016;43:138-148.
2. Schmid-Tannwald C, Oto A, Reiser MF, Zech CJ. Diffusion-weighted MRI of the abdomen: current value in clinical routine. *J Magn Reson Imaging.* 2013;37:35-47.
3. Zhao J, Wang ZJ, Liu M, et al. Assessment of renal fibrosis in chronic kidney disease using diffusion-weighted MRI. *Clin Radiol.* 2014;69:1117-1122.
4. Yildirim E, Kirbas I, Teksam M, Karadeli E, Gullu H, Ozer I. Diffusion-weighted MR imaging of kidneys in renal artery stenosis. *Eur J Radiol.* 2008;65:148-153.
5. Le Bihan D, Breton E, Lallemand D, Aubin ML, Vignaud J, Laval-Jeantet M. Separation of diffusion and perfusion in intravoxel incoherent motion MR imaging. *Radiology.* 1988;168:497-505.
6. Stabinska J, Ljimani A, Zöllner HJ, et al. Spectral diffusion analysis of kidney intravoxel incoherent motion MRI in healthy volunteers and patients with renal pathologies. *Magn Reson Med.* 2021;85:3085-3095.
7. van der Bel R, Gurney-Champion OJ, Froeling M, Stroes ESG, Nederveen AJ, Krediet CTP. A tri-exponential model for intravoxel incoherent motion analysis of the human kidney: in silico and during pharmacological renal perfusion modulation. *Eur J Radiol.* 2017;91:168-174.
8. Periquito JS, Gladytz T, Millward JM, et al. Continuous diffusion spectrum computation for diffusion-weighted magnetic resonance imaging of the kidney tubule system. *Quant Imaging Med Surg.* 2021;11:3098-3119.
9. van Baalen S, Leemans A, Dik P, Lilien MR, Ten Haken B, Froeling M. Intravoxel incoherent motion modeling in the kidneys: comparison of mono-, bi-, and triexponential fit. *J Magn Reson Imaging.* 2017;46:228-239.
10. Ohno N, Miyati T, Kobayashi S, Gabata T. Modified tri-exponential analysis of intravoxel incoherent motion for brain perfusion and diffusion. *J Magn Reson Imaging.* 2016;43:818-823.

11. Hayashi T, Miyati T, Takahashi J, et al. Diffusion analysis with triexponential function in liver cirrhosis. *J Magn Reson Imaging.* 2013;38:148-153.
12. Thiel TA, Valentin B, Ullrich T, et al. Spectral diffusion analysis in patients with high risk for prostate cancer: a feasibility study. *J Magn Reson Med.* 2024. doi:10.1002/jmri.29354
13. Stabinska J, Wittsack HJ, Lerman LO, Ljimani A, Sigmund EE. Probing renal microstructure and function with advanced diffusion MRI: concepts, applications, challenges, and future directions. *J Magn Reson Imaging*. 2023. doi:10.1002/jmri.29127
14. Reischauer C, Gutzeit A. Image denoising substantially improves accuracy and precision of intravoxel incoherent motion parameter estimates. *PLoS One.* 2017;12:e0175106.
15. Gonzalez RC, Woods RE. *Digital Image Processing*. 4th ed. Pearson Education; 2018.
16. Land EH, McCann JJ. Lightness and retinex theory. *J Opt Soc Am.* 1971;61:1-11.
17. Banić N, Lončarić S. Improving the white patch method by subsampling. *Proceedings of the IEEE International Conference on Image Processing (ICIP)*; IEEE; 2014:605-609.
18. Barnard K, Martin L, Coath A, Funt B. A comparison of computational color constancy algorithms. Part II: Experiments with image data. *IEEE Trans Image Process.* 2002;11:985-996.
19. Buades A, Coll B, Morel JM. A review of image denoising algorithms, with a new one. *Multiscale Modeling Simul.* 2005;4:490-530.
20. Stabinska J, Zöllner HJ, Thiel TA, Wittsack HJ, Ljimani A. Image downsampling expedited adaptive least-squares (IDEAL) fitting improves intravoxel incoherent motion (IVIM) analysis in the human kidney. *Magn Reson Med.* 2023;89:1055-1067.
21. Pajevic S, Pierpaoli C. Color schemes to represent the orientation of anisotropic tissues from diffusion tensor data: application to white matter fiber tract mapping in the human brain. *Magn Reson Med.* 1999;42:526-540.
22. Jeurissen B, Tournier JD, Dhollander T, Connelly A, Sijbers J. Multi-tissue constrained spherical deconvolution for improved analysis of multi-shell diffusion MRI data. *Neuroimage.* 2014;103:411-426.
23. Aerts H, Dhollander T, Marinazzo D. Evaluating the performance of 3-tissue constrained spherical deconvolution pipelines for within-tumor tractography. *bioRxiv. 2019;* 629873. doi:10.1101/629873

How to cite this article: Wittsack H-J, Thiel TA, Valentin B, et al. Presentation of microstructural diffusion components by color schemes in abdominal organs. *Magn Reson Med*. 2024;92:2074-2080. doi: 10.1002/mrm.30183